Bismuth iron garnet: *Ab initio* study of electronic properties

Federico Iori,[1] Adrien Teurtrie,[1,2] Laura Bocher,[1] Elena Popova,[2] Niels Keller,[2] Odile Stéphan,[1] and Alexandre Gloter[1]

[1]*Laboratoire de Physique des Solides, CNRS, Univ. Paris-Sud, Université Paris-Saclay, 91405 Orsay Cedex, France*

[2]*Groupe d'Etude de la Matière Condensée (GEMaC), CNRS-UVSQ, Université Paris-Saclay, 78035 Versailles, France*

Bismuth iron garnet (BIG), i.e., $Bi_3Fe_5O_{12}$, is a strong ferrimagnet that also possesses outstanding magneto-optical properties such as the largest known Faraday rotation. These properties are related with the distribution of magnetic moments on octahedral and tetrahedral sites, the presence of spin gaps in the density of state, and a strong spin-orbit coupling. In this work, first-principles *ab initio* calculations are performed to study the structural, electronic, and magnetic properties of BIG using density functional theory with "Hubbard $+ U$" (DFT $+ U$) correction including spin-orbit coupling and HSE06 hybrid functional. We found that the presence of spin gaps in the electronic structure results from the interplay between exchange and correlation effects and the crystal field strengths for tetrahedral and octahedral iron sublattices. The DFT $+ U$ treatment tends to close the spin gaps for larger U due to overlocalization effects, notably in the octahedral site. On the other hand, the hybrid functional confirms the occurrences of three spin gaps in the iron states of the conduction band as expected from optical measurements. A strong exchange splitting at the top of the valence bands associated with a lone-pair type mixture of O p and Bi s, p states is also obtained. Similar exchange splitting was not previously observed for other iron based garnets, such as for yttrium iron garnet. It follows that hole doping, as obtained by Ca substitution at Bi sites, results in a full spin polarized density at the Fermi energy. This work helps to shed more light on the theoretical comprehension of the properties of BIG and opens the route towards the use of advanced many body calculations to predict the magneto-optical coupling effects in BIG in a direct comparison with the experimental measurements.

I. INTRODUCTION

$Bi_3Fe_5O_{12}$ (BIG) is a ferrimagnet insulator exhibiting a magnetoelectric coupling at 300 K, as recently reported [1]. Contrary to its parent structures such as, for example, the well-known yttrium iron garnet (YIG) [2], this material can only be synthesized in thin-film form using nonequilibrium growth techniques [3]. Nevertheless, the growth effort is worth the price since ferrimagnetic bismuth iron garnet shows relatively high magnetization of 1.27×10^5 A/m at 300 K and magnetic ordering temperature from 650 K to 700 K, depending on Bi content and film thicknesses [3,4]. Moreover, BIG giant Faraday rotation effect makes this material a suitable candidate for fast magneto-optical sensors [5], optical isolators [6], and second harmonic generation [7]. Despite the significant technological interest, the structural and electronic properties of BIG thin films remains debated. In literature the preliminary paper of Oikawa and co-workers [8] investigates the electronic structure of BIG through an *ab initio* approach based on spin polarized local density functional theory (LSDA) and full-potential linear combination of atomic orbitals (LCAO) without including any correction treatment for the "correlated" localized 3d electrons.

As known from literature [9,10], local and semilocal functionals suffer from severe delocalization errors [11] particularly relevant for localized d and f electrons. In transition metal oxides, this underestimation can lead to the prediction of metallic band structure instead of the correct insulating one [9]. In the case of BIG this leads to a poor description of the electronic charge density and underestimation of band gaps

and magnetic moments compared to experimental evidences [8]. Recent magneto-optical measurements [3,12,13] reopen the questions regarding the precise description of the spin-dependent electronic structure of BIG. The optical measurements by Kahl [14] in 2003 have reported an optical absorption gap in BIG of 2.3 eV. Recently, Popova and co-workers [1,12] investigated through magneto-optical spectroscopy the spin-dependent electronic density of states (DOS) near and above the Fermi level in BIG. In particular, magneto-optical measurements have revealed a strong asymmetric Faraday hysteresis loop for some photon energies that have been related to the presence of spin gaps in the conduction bands [12].

This work attempts to shed more light on the theoretical description of the electronic and magnetic properties of BIG. In particular, we investigate how the interplay between the treatment of the electronic correlation and the crystal field for the tetrahedral and octahedral sites can modify the spin polarization of the calculated density of states. We also evaluate the influence of the spin-orbit coupling in this density of states. Furthermore, we report an exchange splitting in the top of the valence bands constituted of a mixture of O p, Bi s, and Bi p states typical of a lone pair. Finally, first-principles studies of Ca substituted BIG indicate that a full spin-polarized density at the Fermi energy might be obtained in BIG by doping.

II. METHODS

We have used *ab initio* calculations based on Kohn-Sham density functional theory (DFT) [15,16] in a plane-wave pseudopotential approach as implemented in QUANTUM ESPRESSO

[17]. Scalar and full relativistic ultrasoft pseudopotential, including semicore states and spin-orbit coupling for Bi and Fe, have been obtained from the PSLibrary designed by DalCorso [18]. An energy cutoff of 50 Ry for plane-wave basis expansion and of 400 Ry to describe the charge density and the potential have been respectively used. Geometry has been relaxed at the Gamma k-point until reaching a maximum force on each atom smaller than 10^{-4} eV/Å. Charge density has been converged with $2 \times 2 \times 2$ and $4 \times 4 \times 4$ k points and the density of states with a total mesh of 64 k points in total. We applied a spin-polarized generalized gradient approximation exchange-correlation functional in the Perdew-Burke-Ernzerhof (PBE) [19,20] formulation and, for comparison, in its optimized version for solids (PBEsol) [21]. To improve the treatment of electronic correlation in the description of the correlated subset of Fe d states we apply a "Hubbard $+ U_{eff}$, with $U_{eff} = U - J$" scheme, where U represent the *ad hoc* Hubbard on-site Coulomb repulsion parameter and J the Hund's exchange [22]. We used the effective "Hubbard-U" [23] in the simplified formulation of Cococcioni *et al.* [24] and for spin-orbit calculation the rotationally invariant approach by Liechtestein *et al.* [22]. We evaluate the effect of several values of U keeping the on site Hund's exchange $J = 0$, which formally renders the two approaches equivalent [25] and for the specific case of $U = 4$ eV we checked the effect of the on site exchange by varying J. The U-corrected functionals will thus be referred to as PBE $+ U$ and PBEsol $+ U$. The hybrid functionals have been applied within the HSE06 [26] formulation as implemented in the VASP [27] code.

III. INFLUENCE OF THE HUBBARD CORRECTION

The conventional cell (space group Ia-3d) contains eight chemical formulas for a total of 160 atoms. As yttrium in $Y_3Fe_5O_{12}$ [29–31], the 24 Bi cations of BIG occupy dodecahedral coordinate sites, while the Fe cations are in different coordination sites: 24 tetragonal Fe T_d spin up ($\uparrow$) and 16 octahedral Fe O_h spin down ($\downarrow$), forming two magnetic sublattices ferrimagnetically coupled as shown in Fig. 1(a).

Since the magnetizations of different sublattices do not completely cancel each other, a spontaneous ferrimagnetic polarization rises up. BIG grows only epitaxially in thin film form requiring isostructural garnet substrates, i.e., $Y_3Al_5O_{12}$ (YAG), $Gd_3Ga_5O_{12}$ (GGG), or substituted GGG (SGGG) having smaller lattice constants than that of BIG [12 Å (YAG), 12.37 Å (GGG), and 12.48 Å (SGGG), respectively [32,33]] that result in compressive strain to the BIG film. Therefore, the measurement of the absolute value of the lattice constant remains particularly challenging [33]. In this context, the experimental lattice constant of BIG thin films varies according to literature between 12.60 and 12.633 Å [34–36], while polycrystalline [37] and monocrystalline [38] BIG films have been reported to present slightly larger values of 12.64 or 12.65 Å. We calculated the theoretical lattice a_{theor} constant optimized with PBE $+ U$ and PBEsol $+ U$ for U ranging from 0 to 7 eV and we reported them for comparison in Fig. 1(b).

From Fig. 1(b) it emerges that (i) the PBE and PBEsol theoretical optimized BIG lattice parameters differ from the experimental lattice constant of the garnet substrates by an
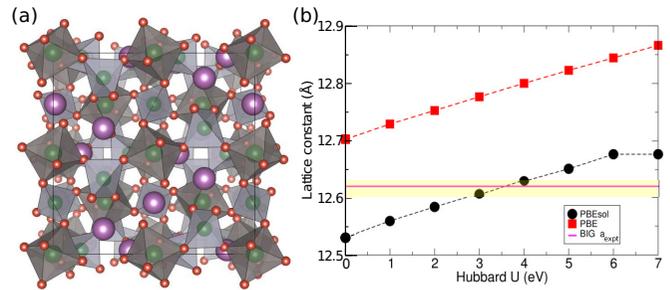

FIG. 1. (a) Conventional crystal structure of bismuth iron garnet with Ia-3d symmetry plotted along [001] direction. Tetragonal (light grsy) and octahedral (dark gray) polyhedra centered on Fe atoms (green) with O atoms (red) at the corners. Bismuth atoms are in violet. Structure plotted with VESTA [28]. (b) Theoretical lattice constants a_{theor} optimized with PBE $+ U$ (red squares) and PBEsol $+ U$ (black dots) as a function of U. The yellow bar indicates the range of variation of the experimental lattice constant and the purple line corresponds to the value $a_{expt} = 12.624$ Å used in this work, as explained in the text.

amount of 1% to 5%, as experimentally observed [33] and (ii) the theoretical lattice constants optimized with PBEsol $+ U$ for U among 2 and 4.5 eV fall into the experimental range of variation indicated by the yellow bar in Fig. 1. An absolute calculation of the BIG lattice constant strongly depends on the exchange-correlation functional used and on the theoretical level of approximation applied to treat the strong electronic correlation effects. To that, hereafter we will choose for our calculations a lattice constant equal to an average value a_{expt} of 12.624 Å, a choice in accordance with previous theoretical studies [8] and with the PBEsol calculation for $U = 4$ eV. Therefore, we will take $U = 4$ eV as the reference value for the Hubbard correction. This choice is also coherent with recent first-principles DFT $+ U$ studies on rare-earth ferrites [29,39–41] and garnets [42], where it has been shown that DTF $+ U = 4$ eV for such oxides permits one to achieve a whole qualitatively and quantitatively consistent description of the structural and electronic properties [43]. The main fingerprints of the electronic structure of BIG are then reported in Table I and Fig. 2. Table I contains the Γ direct electronic gaps [46] and the magnetic moments calculated for both PBE and PBEsol functionals and different Hubbard-U ($U = 0$ and $U = 4$ eV) using a_{expt} lattice constant.

For the same values of U, there are no remarkable differences between the electronic gaps and the magnetic moments obtained by using PBE or PBEsol as shown in Table I. Nonetheless by applying $U = 0$ to 4 eV for both functionals, we get a significant increase of the direct electronic gap E_D (E_D almost doubles to 1.90 eV in PBE $+ U$ and 1.81 eV in PBEsol $+ U$ for a_{expt}) and a slight enhancement of the magnetic moments. Therefore, in our case the change of the electronic gaps and magnetic moments is related to the approximation chosen to treat the electronic correlation rather than to the impact of the lattice parameters. PBE $+ U$ and PBEsol $+ U$ give very close numerical results. The effects of the introduction of electronic correlation are then depicted in Fig. 2, where we show the electronic total density of states (TDOS) and the orbital-projected density of states (PDOS)

TABLE I. Electronic and magnetic properties calculated within PBE $+U$ and PBEsol $+U$ for $U = 0$ and $U = 4$ eV using the average experimental lattice parameter ($a_{\text{expt}} = 12.624$ AA) The first three rows show the direct band gap (E_D), the band gap ($E_\uparrow$) for the spin-up channel, and the band gap ($E_\downarrow$) for the spin-down in eV and calculated at Γk point. The last six rows report the total and iron magnetic moment per formula unit ($\bar{\mu}_{\text{tot}}$, $\bar{\mu}_{\text{Fe}}$) and the moments per atom of each chemical species in units of μ_B.

| | PBE (a_{expt}) | | PBEsol (a_{expt}) | | |
	$U = 0$	$U = 4$	$U = 0$	$U = 4$	Literature
E_D	0.86	1.90	0.77	1.81	2.3[a]
$E_\uparrow$	0.91	1.90	0.83	1.81	2.3[a]
$E_\downarrow$	1.17	2.30	1.11	2.23	2.3[a]
$\bar{\mu}_{\text{tot}}$	3.96	4.00	3.94	3.98	4.25–5.0[b]
$\bar{\mu}_{\text{Fe}}$	2.94	3.09	2.92	3.07	3.45[c]
$\mu_{\text{Fe}(o)}$	−3.51	−3.81	−3.46	−3.80	−3.27[c]
$\mu_{\text{Fe}(t)}$	3.32	3.57	3.28	3.55	3.94[c]
μ_{O}	0.08	0.07	0.08	0.07	0.106[c]
μ_{Bi}	0.002	0.005	0.002	0.005	

[a]Experimental optical gap from Ref. [14].
[b]Experimental value for YIG from Refs. [44,45].
[c]Theoretical values for YIG from Ref. [29].

calculated within PBE (gray) and PBE $+U$ (colored) approximation. With respect to Fig. 2 PBE reproduces an insulating density of states with spectral weight in general agreement with the LSDA calculation by Oikawa [8] but with larger electronic band gaps. The Γ direct gap is 0.86 eV, 0.91 eV for spin-up, and 1.17 eV for spin-down channel (as shown in Table I).
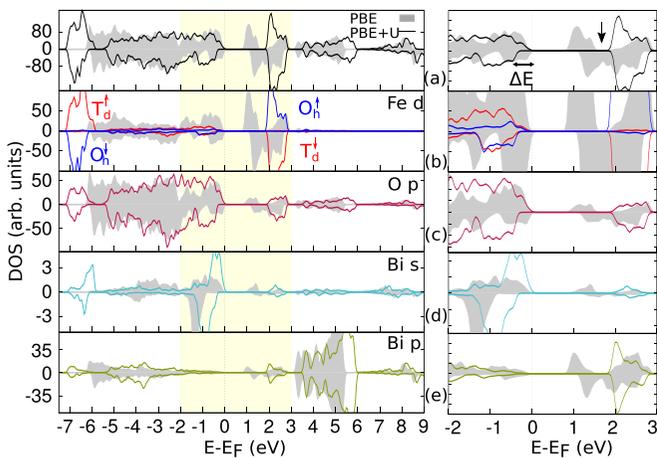

FIG. 2. Total DOS (TDOS) and projected density of states (PDOS) of BIG for PBE in gray filled curve and PBE $+U = 4$ eV in solid line. Left panel shows the overall TDOS and PDOS. Right panel shows the zoom from -2 to 3 eV corresponding to the highlighted part in yellow in the left panel. (a) DOS; PBE in gray, PBE $+U$ in solid line. (b) PDOS of Fe d states: blue curve corresponds to octahedral Fe $O_h^\downarrow$ (filled) and $O_h^\uparrow$ (empty); red curve corresponds to the tetrahedral Fe $T_d^\uparrow$ (filled) and $T_d^\downarrow$ (empty). (c) PDOS of O p states. (d) PDOS of Bi s states, intensity $\times 5$. (e) PDOS of Bi p states.

The PBE projected density of states shows a valence band ranging from 0 to -6 eV characterized by a mixing of O $2p$, Bi $6s$, and Fe $3d$. The PBE conduction states are dominated by the spin-polarized Fe $3d$ in agreement to previous LSDA calculation [8]. The ferrimagnetism in BIG arises clearly from the different spin polarization intensity among the Fe $3d$ electrons in the two Fe T_d and Fe O_h sublattices as shown in Fig. 2(a). Moreover, the crystal-field effects split the Fe $3d$ in a triple degenerate t_{2g} state and in doubly degenerate e_g states with different energetic hierarchy for both sublattices. The clear separation of Fe $3d$ bands for the spin-up conduction band is due to a stronger O_h crystal field. For the minority spin, instead, the T_d crystal field is not strong enough to separate the e_g/t_{2g} contribution in the unoccupied part. This strong difference of crystal field strengths for O_h and T_d symmetry was also experimentally reported in the case of YIG based on the analysis of the d-d optical transitions where crystal field splittings of 1.52 eV and 0.77 eV were derived for respectively O_h and T_d sites [47]. The geometry of the BIG garnet (minority spin in pure O_h site and majority spin in pure T_d site for the occupied band) is at the origin of the 100% spin polarized density of states that occurs at several energies in the DOS calculated by PBE. Indeed the spin-up conduction $O_h^\uparrow$ states are forming two separated peaks centered at 1.2 and 3 eV, while the spin-down $T_d^\downarrow$ states have unique peaks at around 2 eV as reported in Figs. 2(a) and 2(b) by the gray filled curves.

The introduction of the on-site Coulomb interaction Hubbard-U over PBE gives rise to an energy splitting between occupied and empty states in such a way that the former are pushed down and the latter up in energy, as seen in literature for other transition metal oxides and rare-earth garnet [10,42]. In Fig. 2, in colored curves, is shown such PBE $+U$ opening of the band gap followed by the redistribution of spectral weight of the density of states. The O $2p$ states extend from the Fermi energy to ~ -7 eV, but the PBE $+U$ helps to break the hybridization in valence band separating the O $2p$ from the Fe $3d$ states but still showing a non-negligible superexchange character. The top of the valence band around the Fermi level is dominated by the O $2p$ hybridized with Bi $6s$ states. The ferrimagnetic exchange splitting ΔE between spin up and spin down states at the top of the valence band [shown in Fig. 2(a)] is clearly enhanced for $U = 4$ eV and corresponds to 0.36 eV. The interaction between the Bi s, p and the O p orbitals corresponds in our case exactly to the typical "lone pair model" seen in other oxides [48,49]. Indeed, the Bi atoms sit in noncentrosymmetric distorted dodecahedra allowing the mixing of on-site Bi s and Bi p orbitals typical of the lone pair mechanism. According to this model, strong interaction between the Bi s and O p determines the separation in bonding and antibonding states at high energy. This results in the strong contribution of an antibonding Bi s orbital character at the top of the upper valence band. The bottom of conduction has a Fe d character, while the Bi s and p states are upward shifted in energy of almost 1 eV with respect to the PBE calculation. The O $2p$ and Bi $6p$ augment their mutual hybridization between 3.5 eV and 10 eV. The effect of U on the conduction states is more pronounced for the Fe d. The inclusion of Hubbard U on the Fe T_d and Fe O_h states
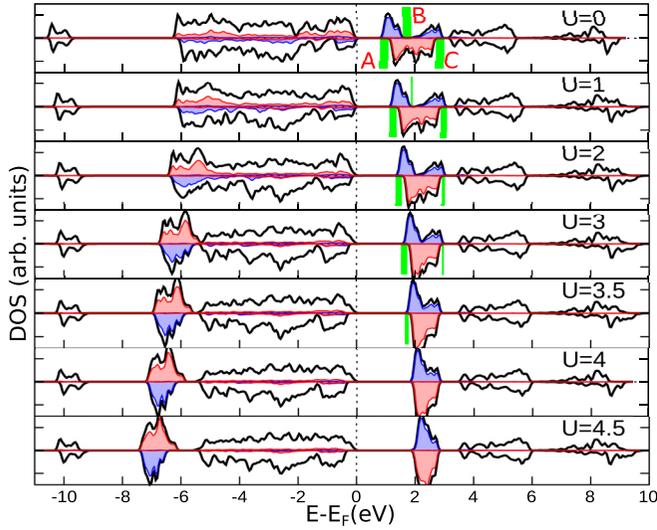
FIG. 3. Evolution of the Fe $3d$ states (Fe O_h in blue and Fe T_d in red) and of the exchange splitting gaps (A,B,C—green lines) among the $O_h^\uparrow$ and the $T_d^\downarrow$ d empty states for Hubbard-U ranging from 0 eV to 4.5 eV. Their values are reported in Table II. The total DOS is reported as reference in solid black line for each U.
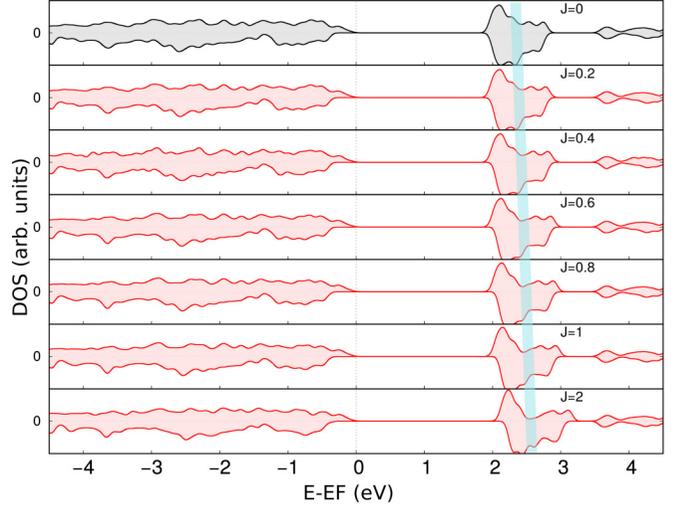

FIG. 4. Effects of Hund's exchange J on the PBE $+ U$-J density of states of BIG for $U = 4$ eV, with J varying from 0 to 2 eV. In the topmost panel (in gray) the calculation of DOS for $J = 0$, corresponding to the PBE $+ U$ DOS shown in Fig. 2. The highlighted cyan window shows the increase of the exchange splitting for $J > 0$.

tends to shrink their bandwidth from 2 to 1.2 eV. The effect is more evident for the $O_h^\uparrow$ states where the $t_{2g} - e_g$ splitting (indicated for the $U = 0$ calculation by the black arrow in Fig. 2) disappears.

In order to interpret the spin gap closure of the $O_h^\uparrow$ states we have evaluated the effects of Hubbard U on the O_h and T_d crystal field splitting for U ranging from 0 eV to 4.5 eV as shown in Fig. 3 and reported in Table II. For increasing value of U the $3d$ states change completely their energy position. In valence band the Fe states spectral weight is depleted from the Fermi level and shifted downward in energy with an important reduction of the hybridization between the O and Fe orbitals. For $U = 4$ eV, the Fe majority occupied states $T_d^\uparrow$ and the minority spin $O_h^\downarrow$ form two antiferrimagnetic peaks centered around -7 eV of Fermi energy (FE) that become separated from the main oxygen band. With increasing the value of U,

TABLE II. PBE $+ U$ electronic gaps and magnetic moments as a function of U. The total band gap E_g is calculated as the energy difference between the lowest energy conduction state and the highest energy valence state at the Γ k point; A,B,C are the exchange gaps in the conduction density of states as shown in Fig. 3. The magnetic moments μ are calculated per formula unit (f.u.).

U	E_g (eV)	A (eV)	B (eV)	C (eV)	μ/f.u. (μ_B)	μ_{Fe}/f.u. (μ_B)
0	0.91	0.31	0.20	0.25	3.96	2.40
1	1.19	0.29	0.10	0.25	3.97	3.98
2	1.42	0.27		0.15	3.98	3.01
3	1.66	0.23		0.24	3.98	3.04
4	1.90	0.05			4.00	3.09
5	1.91	0.07			4.00	3.15
6	1.77	0.11			4.02	3.2

it is noteworthy that the top of the valence band also becomes spin split.

In the conduction band the principal effect of U is to reduce the bandwidth of both spin-up and spin-down Fe $3d$. The main effect is the disappearance of the gap between the spin-up O_h states present in the PBE calculation (indicated by the black arrow in Fig. 2 and B in Fig. 3). This closure is linear with U and it appears clearly at $U = 3$ eV with a transition in DOS from a structure with two peaks to a structure with only one well-defined peak. The localization effects of the Hubbard term is stronger for the spin-up composed of O_h symmetry with larger hybridization than for the spin-down with pure T_d contribution. At moderate (for a transition metal oxide) value of U, the spin gaps observed at the three energies A,B,C (reported in Fig. 3) in the DOS tend to disappear, while magneto-optic measurements have revealed the existence of several spin gaps [12]. On the contrary, the total and the Fe magnetic moments per formula units are almost stabilized for different U values around $\mu = 3\mu_B$ and $\mu = 4\mu_B$, respectively. The Hubbard term therefore aims to correct the delocalization error of pure DFT-PBE, but seems to induce a spurious artifact in the correct description of the hybridization between oxygen and the iron states [43]. We then take into account the effect of the Hund's exchange J by performing a fully rotationally invariant PBE $+ U_{eff}$ calculation [50]. For fixed $U = 4$ eV we varied J and monitored the evolution of electronic and magnetic properties. In Fig. 4 is reported the evolution of the total DOS for PBE $+ U_{eff}$, for J ranging from 0 to 2 eV. We can see that, for $J > 0$, the exchange splitting among the conduction Fe d states increases progressively (cyan highlighted region in Fig. 4) as observed in similar work in the literature [51]. The electronic Γ direct gap is increasing between 1.90 eV for $J = 0$ and 2 eV for $J = 2$ eV, while the Fe magnetic moments $\mu_{Fe(o)}$ and $\mu_{Fe(t)}$ are stabilized around $-4\mu_B$ and $3.8\mu_B$, respectively. Interestingly, for $J = 2$ eV the huge exchange splitting among the Fe d counteracts the
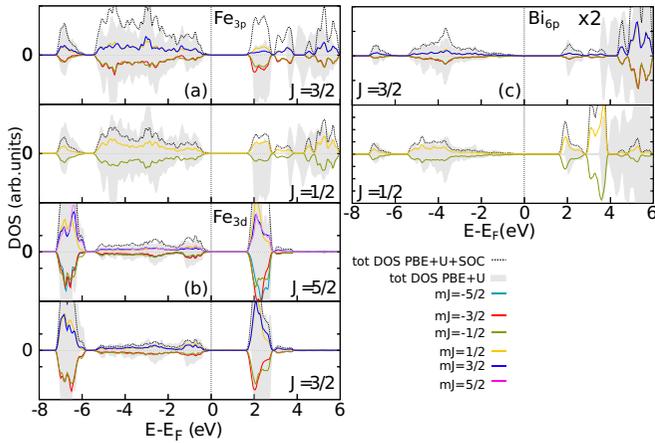
FIG. 5. PDOS $PBE + U + SOC$ and $PBE + U$ spin polarized cases. In (a) the Fe $3p$, in (b) the Fe $3d$, and in (c) the Bi $6p$. In each panel $PBE + U$ DOS is in gray; the total $PBE + U + SOC$ DOS is in dotted black line. The total l-resolved DOS per element (dotted black line) is the sum of all the corresponding m_J projections (solid colored lines). The intensity of the Bi $6p$ has been magnified by 2.
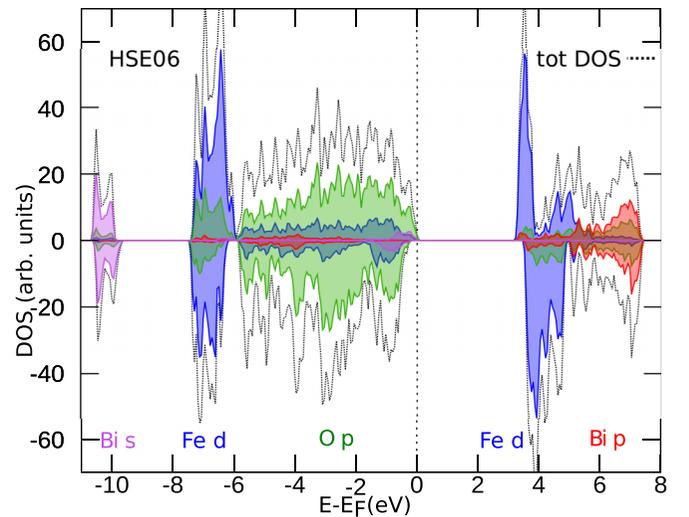

FIG. 6. HSE06 hybrid functional calculation of the TDOS and PDOS. The different projected angular moment channels shown correspond to Bi $6s$ in lilac, Fe $3d$ in blue, O $2p$ in green, and Bi $6p$ in red. For sake of computational cost we have adopted here the 80-atoms rhombohedral primitive cell of BIG with a_{expt} lattice constant [55].

overlocalization observed for $PBE + U$, $U = 4$ eV permitting one to recover the octahedral crystal field splitting and an almost full spin polarization behavior in the conduction states.

Moreover, the role of the spin-orbit (SO) coupling of the bismuth and iron atoms on the density of states of the BIG has been evaluated. In Fig. 5 are compared the atom-projected $PBE + U$ density of states with the $PBE + U + SOC$ density of states projected for different values of the moment m_J. The SOC affects mainly the Bi $6p$ and only slightly the Fe $3p$ and Fe $3d$.

As compared to the $PBE + U$ calculations where the Bi p main states were spanning from 3 to 6 eV, the $PBE + U + SOC$ calculated DOS results in a Bi $(6p_{1/2})$ spanning from 2 to 4 eV and the Bi $(6p_{3/2})$ from 4 to 7 eV. The Fe $3p$ and Fe $3d$ states are then more hybridized with the bismuth when SOC is included via the Bi $(6p_{1/2})$ states. The SO effect on iron d states is instead very soft. In the Fe $3d$ valence band the SO splitting is 50 meV, while in conduction it is around 25 meV, in good agreement with experimental and calculated values reported by Oikawa [8].

IV. HYBRIDS FUNCTIONAL APPLIED TO BIG

We have also calculated the electronic structure with HSE06 hybrid functional on top of PBE as implemented in VASP [27]. HSE06 improves the electronic structure description and the correct orbital occupation beyond a local or semilocal approximation stemming from treating all the electrons on the same footing [10,52,53]. This hybrid functional can be considered one of the best static nonlocal approaches to GW approximation in order to reproduce band gap and optical dielectric functions close to experiments [9,54]. For instance, hybrid functional applied to iron oxides have successfully reproduced the electronic structure of LaFeO$_3$ [56]. In particular, the energy separation of unoccupied t_{2g} and e_g states have been demonstrated to be almost independent of the amount

of Hartree-Fock exchange and to be in good agreement with x-ray absorption spectroscopy and GW calculation.

The use of PBE-HSE06 hybrid functional is then expected to be more accurate for the calculation of crystal field split bands. The PBE-HSE06 total and projected DOS of BIG are shown in Fig. 6. Interestingly, the hybrid functional preserves the strong splitting of the octahedral crystal field and thus the full spin polarized regions of the unoccupied states.

Moreover, as seen for other oxides, the nonlocal Fock exchange part contained in the HSE06 increases the band gap by an upward energy shift of the empty states with respect to $PBE + U$, as shown in Table III: The HSE06 band gap is now 3.23 eV against the 2.04 eV of $PBE + U$. However, the effect of the hybrid functional is very similar to the $PBE + U$-J calculation shown in Fig. 4. Both approaches increase the exchange splitting in the conduction d states, stabilizing the Fe magnetic moments around the experimental values and opening the electronic band gap closer to more reasonable values. To that we can say that once more the exchange

TABLE III. PBE-HSE06 and $PBE + U$ band gaps and magnetic moments calculated with VASP with a_{expt}. E_g is the total band gap direct at Γ k point.

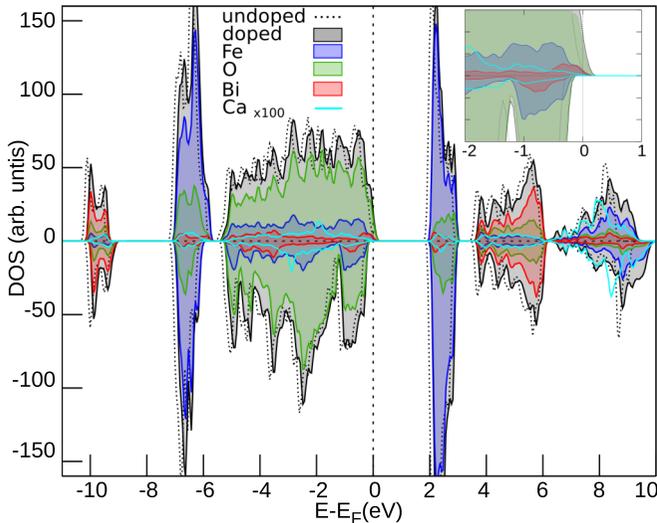|	E_g (eV)	μ/f.u. (μ_B)	μ_{Fe}/f.u. (μ_B)
$U = 0$	0.85	4.31	3.34
$U = 4$	2.04	4.47	3.68
$U = 5$	2.32	4.50	3.75
$U = 6$	2.53	4.54	3.83
$U = 7$	2.67	4.59	3.91
$U = 8$	2.77	4.60	3.98
HSE06	3.23	4.48	3.64

FIG. 7. PBE + U (U = 4 eV) total and projected DOS of BIG Ca-doped calculated with QUANTUM ESPRESSO. (Ca projected DOS has been magnified by 100). The dotted black line corresponds to the undoped pristine BIG total DOS, while the Ca-doped total DOS is in gray. The inset shows a magnification around the Fermi energy between −2 and 1 eV.

effects have to be seriously considered too when dealing with correlated oxides.

HSE06 hybrid functional is known to generally overestimate the band gap [9]. The HSE06 gap of 3.23 eV can be then considered as a superior limit for the electronic band gap value of BIG. The presence of a strong exciton in optical spectra would therefore reduce the electronic gap below the value of 3.23 eV. This is therefore compatible and coherent with the experimental optical gap of 2.3 eV measured by Kahl [14] and then confirmed recently by Deb [12]. Hence in absence of photoemission measurements we can infer that the real electronic band gap of BIG should be included between 2 and 3 eV for a crystal structure associated with a_{expt} = 12.624 Å. Moreover, HSE06 confirms a substantial exchange splitting at the top part of the valence band and at −10 eV of the Bi s states as we found for the PBE + U calculations. The total and iron magnetic moments per f.u. remain also similar to the values obtained by PBE + U. The use of the hybrid functional gives similar results as the PBE + U-J calculation shown in Fig. 4. Both approaches increase the exchange splitting in the conduction d states, stabilizing the Fe magnetic moments around the experimental values and opening the electronic band gap closer to more reasonable values. The inclusion of a substantial amount of exchange interaction is then primordial to obtain the correct ground state in these iron garnets. The relatively strong exchange splitting of the top of the valence band is a key figure of the BIG electronic structure and is not present in the calculated YIG electronic structure [57]. The top of the valence band is mostly composed of Bi s and O p and such spin-splitting might be of importance for

magneto-optic excitations where p-d transitions are allowed or for electric transport to obtain a high spin polarization in the presence of impurities. In the specific case of hole doping, this could lead to a Fermi level with a strong spin polarization. We performed calculations with a calcium substituted to a Bi atom corresponding to a doping concentration of 4%. In Fig. 7 are reported the total and projected DOS of undoped and Ca-doped BIG calculated within PBE + U. The calcium atom, stabilized in its divalent state, gives rise to an hole doping and an almost 100% spin polarized density of states observed at the Fermi level. At that concentration, no impurity band is formed in the band gap and the nonzero density of states crossing the Fermi level indicates that Ca-doped BIG is now a metal due to the hole doping. The character of the band at the Fermi level is mostly made of O p orbitals for such concentration. Nonetheless, the Ca-doped BIG appears then as a possible candidate for obtaining a full spin polarized ligand hole electronic structure.

V. CONCLUSION

To conclude, the occurrence of spin gaps in the Fe $3d$ states of the conduction band due to the difference of crystal field value for O_h and T_d sites is observed by PBE, PBE + U for a limited range of U values and by the hybrid functional HSE06 conforming the presence of spin gaps as derived from optical measurements [12]. The disappearance of the spin gaps at large U values is certainly due to some overlocalization effect of the PBE + U approach that mostly alters the O_h sites. The inclusion of spin orbit coupling mostly changes the unoccupied DOS resulting at lower energy of a Bi p (j = 1/2) hybridized with Fe states and at higher energy of Bi p(j = 3/2) states. The upper part of the valence band is composed of O p and Bi s states and has also a strong spin polarization that was not reported for YIG. The band gap obtained by HSE06 gives an E_g of ∼3.2 eV that can be considered an upper limit reference for the electronic and optical one. For future outlooks, this work helps to shed more light on the theoretical comprehension of the properties of BIG and opens the route towards the use of advanced many body calculations [58] to correctly predict the magneto-optical coupling effects in BIG in a direct comparison with the experimental measurements.

[1] E. Popova, A. Shengelaya, D. Daraselia, D. Japaridze, S. Cherifi-Hertel, L. Bocher, A. Gloter, O. Stéphan, Y. Dumont, and N. Keller, Appl. Phys. Lett. **110**, 142404 (2017).

[2] E. Popova, N. Keller, F. Gendron, M. Guyot, M.-C. Brianso, Y. Dumond, and M. Tessier, J. Appl. Phys. **90**, 1422 (2001).

[3] B. Vertruyen, R. Cloots, J. S. Abell, T. J. Jackson, R. C. da Silva, E. Popova, and N. Keller, Phys. Rev. B **78**, 094429 (2008).

[4] E. Popova, A. F. F. Galeano, M. Deb, B. Warot-Fonrose, H. Kachkachi, F. Gendron, F. Ott, B. Berini, and N. Keller, J. Magn. Magn. Mater. **335**, 139 (2013).

[5] P. Görnert, A. Lorenz, M. Lindner, and H. Richert, in *Crystal Growth Technology*, edited by P. Capper and P. Rudolph (John Wiley & Sons, Ltd, 2010), Chap. 14, pp. 249–266.

[6] S. M. Drezdzon and T. Yoshie, Opt. Express **17**, 9276 (2009).

[7] P. Kumar, A. I. Maydykovskiy, L. Miguel, N. V. Dubrovina, and O. A. Aktsipetrov, Opt. Express **18**, 1076 (2010).

[8] T. Oikawa, S. Suzuki, and K. Nakao, J. Phys. Soc. Jpn. **74**, 401 (2005).

[9] F. Iori, M. Gatti, and A. Rubio, Phys. Rev. B **85**, 115129 (2012).

[10] C. Rödl, F. Fuchs, J. Furthmüller, and F. Bechstedt, Phys. Rev. B **79**, 235114 (2009).

[11] P. Mori-Sánchez, A. J. Cohen, and W. Yang, Phys. Rev. Lett. **100**, 146401 (2008).

[12] M. Deb, E. Popova, A. Fouchet, and N. Keller, Phys. Rev. B **87**, 224408 (2013).

[13] B. Koene, M. Deb, E. Popova, N. Keller, T. Rasing, and A. Kirilyuk, Phys. Rev. B **91**, 184415 (2015).

[14] S. Kahl, V. Popov, and A. M. Grishin, J. Appl. Phys. **94**, 5688 (2003).

[15] W. Kohn and L. J. Sham, Phys. Rev. **140**, A1133 (1965).

[16] P. Hohenberg and W. Kohn, Phys. Rev. **136**, B864 (1964).

[17] P. Giannozzi, S. Baroni, N. Bonini, M. Calandra, R. Car, C. Cavazzoni, D. Ceresoli, G. L. Chiarotti, M. Cococcioni, I. Dabo, A. D. Corso, S. de Gironcoli, S. Fabris, G. Fratesi, R. Gebauer, U. Gerstmann, C. Gougoussis, A. Kokalj, M. Lazzeri, L. Martin-Samos *et al.*, J. Phys.: Condens. Matter **21**, 395502 (2009).

[18] A. D. Corso, Comput. Mater. Sci. **95**, 337 (2014).

[19] J. P. Perdew, K. Burke, and M. Ernzerhof, Phys. Rev. Lett. **77**, 3865 (1996).

[20] U. von Barth and L. Hedin, J. Phys. C: Solid State Phys. **5**, 1629 (1972).

[21] J. P. Perdew, A. Ruzsinszky, G. I. Csonka, O. A. Vydrov, G. E. Scuseria, L. A. Constantin, X. Zhou, and K. Burke, Phys. Rev. Lett. **100**, 136406 (2008).

[22] A. I. Liechtenstein, V. I. Anisimov, and J. Zaanen, Phys. Rev. B **52**, R5467(R) (1995).

[23] S. L. Dudarev, G. A. Botton, S. Y. Savrasov, C. J. Humphreys, and A. P. Sutton, Phys. Rev. B **57**, 1505 (1998).

[24] M. Cococcioni and S. de Gironcoli, Phys. Rev. B **71**, 035105 (2005).

[25] P. Baettig, C. Ederer, and N. A. Spaldin, Phys. Rev. B **72**, 214105 (2005).

[26] J. Heyd, G. E. Scuseria, and M. Ernzerhof, J. Chem. Phys. **118**, 8207 (2003).

[27] G. Kresse and J. Furthmüller, Phys. Rev. B **54**, 11169 (1996).

[28] K. Momma and F. Izumi, J. Appl. Crystallogr. **44**, 1272 (2011).

[29] W. Y. Ching, Z. quan Gu, and Y.-N. Xu, J. Appl. Phys. **89**, 6883 (2001).

[30] C. Suchomski, C. Reitz, C. T. Sousa, J. P. Araujo, and T. Brezesinski, Chem. Mater. **25**, 2527 (2013).

[31] S. Geller, H. J. Williams, G. P. Espinosa, R. C. Sherwood, and M. A. Gilleo, Appl. Phys. Lett. **3**, 21 (1963).

[32] S. Kahl, S. I. Khartsev, A. M. Grishin, K. Kawano, G. Kong, R. A. Chakalov, and J. S. Abell, J. Appl. Phys. **91**, 9556 (2002).

[33] E. Popova, M. Deb, L. Bocher, A. Gloter, O. Stéphan, B. Warot-Fonrose, B. Berini, Y. Dumont, and N. Keller, J. Appl. Phys. **121**, 115304 (2017).

[34] N. Adachi, V. P. Denysenkov, S. I. Khartsev, A. M. Grishin, and T. Okuda, J. Appl. Phys. **88**, 2734 (2000).

[35] M. Okada, S. Katayama, and K. Tominaga, J. Appl. Phys. **69**, 3566 (1991).

[36] T. Okuda, T. Katayama, H. Kobayashi, N. Kobayashi, K. Satoh, and H. Yamamoto, J. Appl. Phys. **67**, 4944 (1990).

[37] H. Toraya and T. Okuda, J. Phys. Chem. Solids **56**, 1317 (1995).

[38] S. Mino, M. Matsuoka, A. Tate, A. Shibukawa, and K. Ono, Jpn. J. Appl. Phys. **31**, 1786 (1992).

[39] O. Diéguez, O. E. González-Vázquez, J. C. Wojdeł, and J. Íñiguez, Phys. Rev. B **83**, 094105 (2011).

[40] C. Xu, Y. Yang, S. Wang, W. Duan, B. Gu, and L. Bellaiche, Phys. Rev. B **89**, 205122 (2014).

[41] J. B. Neaton, C. Ederer, U. V. Waghmare, N. A. Spaldin, and K. M. Rabe, Phys. Rev. B **71**, 014113 (2005).

[42] R. Nakamoto, B. Xu, C. Xu, H. Xu, and L. Bellaiche, Phys. Rev. B **95**, 024434 (2017).

[43] J. K. Shenton, D. R. Bowler, and W. L. Cheah, J. Phys.: Condens. Matter **29**, 445501 (2017).

[44] H. Pascard, Phys. Rev. B **30**, 2299 (1984).

[45] D. Rodic, M. Mitric, R. Tellgren, H. Rundlof, and A. Kremenovic, J. Magn. Magn. Mater. **191**, 137 (1999).

[46] Our band structure calculated with and without SOC (here not shown) give evidence of a Γ direct band gap in agreement with the few DFT calculations from literature [8].

[47] A. G. Gavriliuk, V. V. Struzhkin, I. S. Lyubutin, and I. A. Trojan, JETP Lett. **82**, 603 (2005).

[48] A. Walsh and G. W. Watson, Chem. Mater. **19**, 5158 (2007).

[49] A. Walsh, D. J. Payne, R. G. Egdell, and G. W. Watson, Chem. Soc. Rev. **40**, 4455 (2011).

[50] S. Keshavarz, J. Schött, A. J. Millis, and Y. O. Kvashnin, Phys. Rev. B **97**, 184404 (2018).

[51] H. Chen and A. J. Millis, Phys. Rev. B **93**, 045133 (2016).

[52] C. Franchini, J. Phys.: Condens. Matter **26**, 253202 (2014).

[53] M. Choi, A. Janotti, and C. G. Van de Walle, Phys. Rev. B **88**, 214117 (2013).

[54] M. A. L. Marques, J. Vidal, M. J. T. Oliveira, L. Reining, and S. Botti, Phys. Rev. B **83**, 035119 (2011).

[55] Charge density has been converged with $4 \times 4 \times 4$ k-points mesh. We used a plane-wave energy cutoff of 500 eV and projected augmented wave (PAW) pseudopotential [59] as implemented in VASP [27]. For PBE + U we tested the equivalence of the rotationally invariant approach introduced by Liechtenstein [22] and the simplified (rotationally invariant) approach by Dudarev [23] imposing $J = 0$.

[56] J. He and C. Franchini, Phys. Rev. B **86**, 235117 (2012).

[57] Y.-N. Xu, Z.-q. Gu, and W. Y. Ching, J. Appl. Phys. **87**, 4867 (2000).

[58] D. Sangalli, A. Marini, and A. Debernardi, Phys. Rev. B **86**, 125139 (2012).

[59] G. Kresse and D. Joubert, Phys. Rev. B **59**, 1758 (1999).